Journal of Electronic Research and Application, 2026, Volume 10, Issue 3
http://ojs.bbwpublisher.com/index.php/JERA
ISSN Online: 2208-3510
ISSN Print: 2208-3502

Experimental Investigation of the Velocity Distribution in the Tail Flame of an Inductively-Coupled-Plasma

Xiaobao Mao

China West Normal University, Nanchong 637002, Sichuan, China

Abstract: To achieve an accurate description of an Inductively Coupled Plasma (ICP) source, numerous two-dimensional and three-dimensional numerical models have been developed. However, experimental validation of these models remains a major challenge. Compared with plasma temperature and electron number density, the measured gas flow velocity distribution is more direct and reliable, and can serve as an important criterion for assessing model validity. In this work, the experimental method was improved by optimizing the observation parameters of a high-speed camera, effectively suppressing the interference from the intense emission spectra in the normal analytical zone. For the first time, ion clouds formed by injected particles were directly observed. Five types of suspended particles were sequentially introduced, including Er_2O_3, Y_2O_3, and borosilicate glass particles with diameters of 10, 5, and 2 μm. The particle-flow following behavior was comparatively evaluated. Using a tracer method, the gas flow velocity distribution in the ICP tail plume was measured. Furthermore, with Y_2O_3 as the tracer, the axial gas velocity distribution in the central channel was systematically measured under different radio-frequency (RF) powers and carrier gas flow rates. The results show that within the range of 2.5 mm < z < 12.5 mm, the axial gas velocity in the central channel of the tail plume exhibits a distinct plateau region. The axial gas velocity increases with increasing RF power, while showing weak sensitivity to variations in carrier gas flow rate. The present study provides experimental data on the axial gas velocity distribution, offering essential validation and correction benchmarks for numerical ICP models.

Keywords: Inductively coupled plasma; Axial velocity distribution; Ar-ICP; High-speed camera

Online publication: April 22, 2026

1. Introduction

Inductively coupled plasma (ICP) sources, as crucial energy sources and ion sources, are widely used in analytical instruments such as Inductively Coupled Plasma Mass Spectrometry (ICP-MS) and Inductively Coupled Plasma Optical Emission Spectrometry (ICP-OES) [1,2]. For ICP sources intended for analytical purposes, fundamental research typically focuses on the spatial distribution characteristics of internal plasma parameters (e.g., electron

temperature, ion temperature, gas flow velocity) and their main influencing factors. The relevant research methods are mainly divided into two categories: experimental diagnostics and numerical simulation. In terms of numerical simulation, two-dimensional axisymmetric models based on commercial software platforms such as ANSYS Fluent and COMSOL Multiphysics are now relatively mature and can effectively describe the fundamental behavior of the plasma. However, these two-dimensional models have significant limitations when dealing with actual three-dimensional complex structures, such as accurately representing the geometric asymmetry of the actual torch and load coil, the three-dimensional flow effects caused by the tangential injection of the cooling gas, and the entrainment and mixing process between the plasma and the surrounding gas. Consequently, in recent years, several research teams have successively conducted three-dimensional numerical simulation studies, aiming to more realistically reflect the underlying physical and chemical processes [3–6]. Nevertheless, systematic experimental validation of three-dimensional simulation results remains relatively scarce. Common validation methods primarily focus on two aspects: one is the qualitative or quantitative comparison of the simulated flow field structure with plasma vortex morphology observed using custom-built ICP sources equipped with high-speed cameras or schlieren systems; the other is the comparison of simulated plasma parameters (e.g., temperature, velocity) with two-dimensional distribution data obtained via diagnostic techniques such as optical emission spectroscopy, laser Thomson scattering, or Rayleigh scattering [3,4,7,8]. While these comparative efforts provide important foundations for model validation, the development of more comprehensive and refined three-dimensional experimental diagnostic methods is still necessary to enhance the reliability and predictive capability of simulation results.

Previous studies have employed various optical and time-resolved diagnostic techniques to experimentally measure the flow velocity distribution inside the ICP torch and within the normal analytical zone, primarily including high-speed photography, Particle Image Velocimetry (PIV), and Time-of-Flight (TOF) methods [9–12]. Due to the intense continuous emission background in the upstream region of the Normal Analytical Zone (NAZ, < 20 mm above the load coil), the signal from ion clouds is difficult to extract effectively. Consequently, reliable experimental data on the velocity distribution in this region are still lacking. Overall, systematic flow velocity measurement data covering the complete space from the torch exit to the downstream region for the same ICP device remain very limited, which hinders the comprehensive validation and further optimization of current ICP numerical models.

This work conducts a systematic experimental investigation of the normal analytical zone of an ICP based on a custom-built ICP device. By optimizing the observation parameters of a high-speed camera, ion clouds from sampled particles were directly observed, and the flow velocity distribution of the pure argon plasma was obtained. By varying the plasma RF power and sample gas flow rate, the corresponding gas flow velocity distributions were measured. The results were compared with simulations from a previously established two-dimensional numerical model to validate the experimental data and elucidate the flow mechanisms.

2. Experimental methodology

2.1. Experimental apparatus and reagents

The experimental setup consists of an RF generator, an impedance matching network, a load coil, a micro nebulizer, and a cyclonic spray chamber. The flow rates of the coolant, auxiliary, and sample gases are precisely controlled by mass flow controllers, and high-purity argon (99.999%) is used. Unless otherwise specified, the ICP

operating conditions were set to W, L/min, L/min, and L/min. The schematic diagram of the system is shown in **Figure 1**.

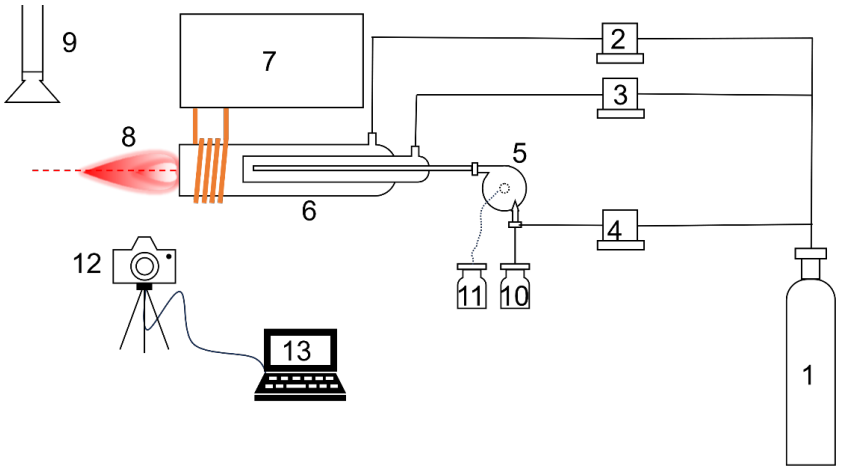

Figure 1. Schematic diagram of the facility (1: Argon gas cylinder, 2: MFC for coolant gas, 3: MFC for auxiliary gas, 4: MFC for sample gas, 5: Nebulizer and cyclone chamber, 6: Quartz torch, 7: r.f. power generator and impedance matching network, 8: Plasma, 9: Exhaust pipe, 10: Suspension sample, 11: Waste, 12: High-speed colour camera, 13: Computer).

Five types of particulate samples were used in this study, including ground Er_2O_3 and Y_2O_3 oxide powders, and borosilicate glass particles with nominal diameters of approximately 10, 5, and 2 μm (denoted as BSG_10, BSG_5, and BSG_2, respectively). The particle size and morphology were examined using a digital microscope. The powders were dispersed and diluted in ultrapure water to prepare suspensions of appropriate concentrations for analysis. To facilitate comparison of the aerodynamic behavior of different particles, their aerodynamic diameters were calculated according to:

$$D_a = D_p\sqrt{\rho} \quad (1)$$

where (D_p) is the geometric particle diameter and (ρ) is the particle material density.

As shown in **Table 1**, the aerodynamic equivalent diameters of these particles range from 3.3 to 35 μm, which is sufficient to evaluate their ability to follow the gas flow.

Table 1. Summary of particles used for flow tracking

No.	Name	Dno/μm	Dp/μm	ρ/g cm-3	Da/μm	Source
1	Er_2O_3 powder	/	11.78	8.64	34.63	Self-grinded
2	Y_2O_3 powder	/	9.53	5.03	21.37	
3	BSG_10	10.2	10.73	2.55	17.14	
4	BSG_5	4.6	5.48	2.55	8.75	Thermo Fisher
5	BSG_2	2.0	2.11	2.50	3.34	
/	Graphite powder	/	9.41	2.27	14.18	Guo *et al.* 2019

2.2. Measurement of plasma tail flame velocity with different sampled particles

To investigate the influence of particle physical properties on ICP tail flame velocity measurements, suspensions

containing different particles were sequentially nebulized under fixed RF power and carrier gas flow conditions. After entering the plasma, the particles underwent heating, evaporation, and ionization, forming luminous particle clusters. A color high-speed camera (75,000 fps, 1280 × 144 pixels) was used to record their motion. By optimizing the aperture and exposure time, high signal-to-noise particle trajectory images were obtained. **Figure 2** shows four consecutive frames captured in the central channel during nebulization of a Y_2O_3 suspension at 1200 W RF power and 1.0 L/min carrier gas flow rate. The bright streaks correspond to the trajectories of individual particle clusters during the exposure time. Using this approach, the particle tracing method was applied to determine the velocity distribution in the Ar-ICP tail flame.

Figure 2. High-speed images showing the motion trajectories of Y_2O_3 particles in the central channel of the plasma.

3. Results and discussion

3.1. Influence of camera aperture and shutter speed on ICP tail flame imaging

In previous studies, the aperture and shutter parameters of the high-speed camera were not systematically optimized, resulting in excessive brightness of the ICP tail flame near the torch exit, which made it difficult to obtain reliable velocity distribution data in this region. To reduce the tail flame signal intensity and achieve clear imaging of the normal analytical zone near the torch outlet, the imaging conditions were optimized by carefully adjusting the camera aperture and shutter settings. The aperture controls the amount of incident light, whereas the shutter determines the exposure time. After stable plasma ignition, transient images of the tail flame under pure argon (Ar) conditions were recorded using a color high-speed camera (MEMRECAM ACS-3, NAC Co., Japan). By systematically varying the aperture-shutter combinations, clear images of the plasma in the central channel were successfully obtained.

To investigate the effect of aperture on tail flame imaging, the shutter time was fixed at 20 μs while the aperture setting was varied. The results are shown in **Figure 3**. The image brightness increased significantly with increasing aperture number, indicating that the aperture setting effectively reflects the degree of aperture opening.

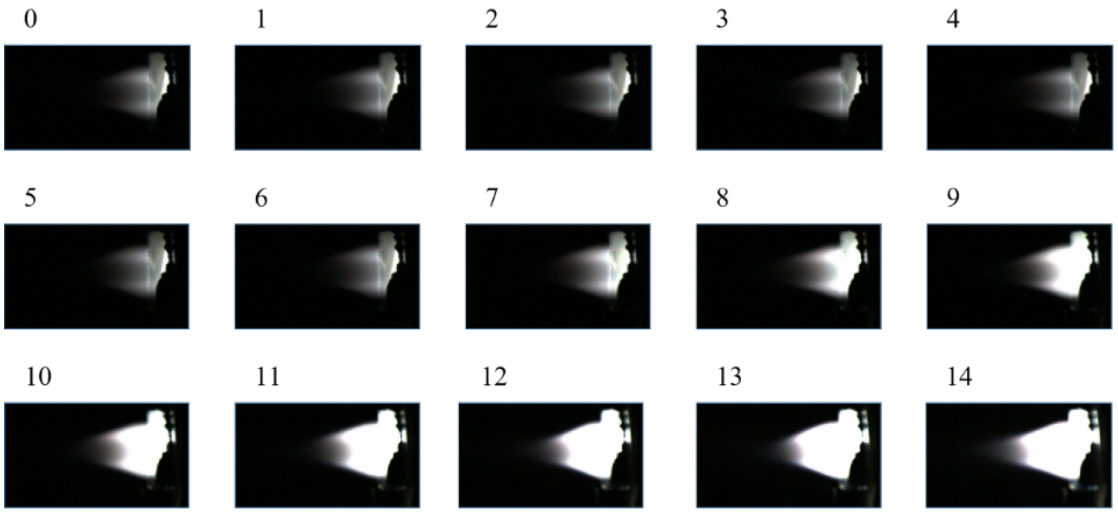

Figure 3. The pictures of pure Ar-ICP captured by the camera operating at 20μs shutter duration and varying apertures. The number represents the aperture index.

To investigate the effect of shutter speed on tail flame imaging, the camera aperture was fixed at setting 0, and the shutter time was sequentially adjusted to 10, 20, 30, 40, 50 , and 62 μs (maximum value). The results are shown in **Figure 4**. The image brightness increased significantly as the shutter speed decreased, indicating that longer exposure times resulted in stronger collected light signals.

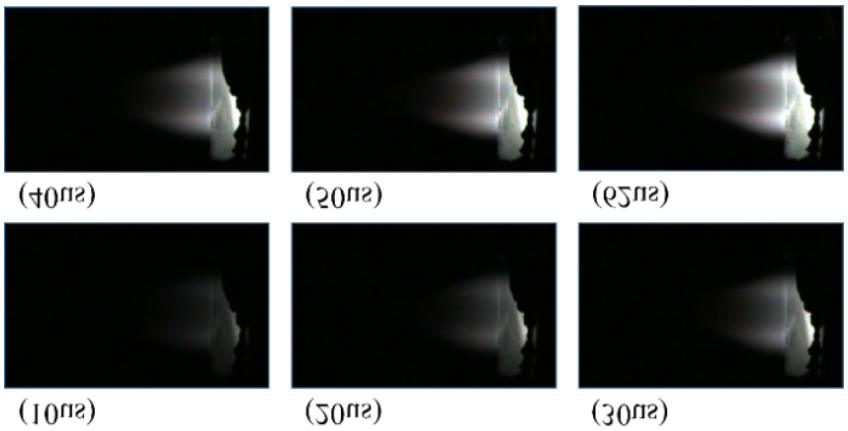

Figure 4. The pictures of pure Ar-ICP captured by the camera operating at aperture "0" and varying shutter duration. The number indicates the shutter value.

Since both the camera aperture and shutter speed affect the image brightness near the torch outlet, coordinated adjustment of these two parameters is required when imaging the tail flame. To clearly capture the plasma central channel at the torch exit and obtain high-contrast images of particle trajectories, the aperture-shutter combinations were systematically optimized. Several parameter settings suitable for central channel visualization were ultimately identified. **Figure 5** shows representative examples of aperture and shutter combinations that clearly reveal the plasma central channel.

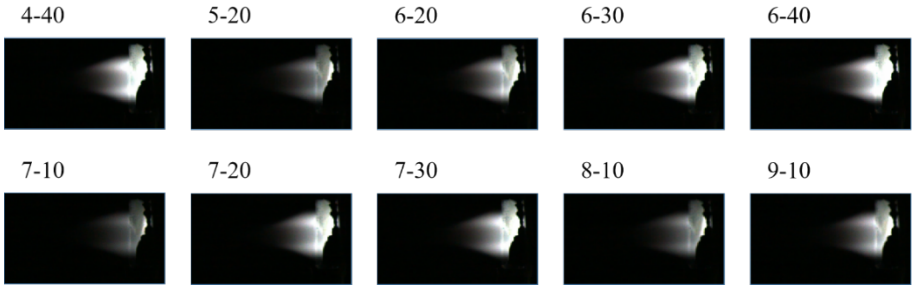

Figure 5. Morphology of the pure Ar-ICP tail flame under different aperture and shutter settings (labels indicate aperture number-shutter time combinations).

3.2. Influence of different particles on ICP tail flame velocity distribution measurements

The suspension containing Er_2O_3 powder was first introduced into the ICP torch via nebulization through the carrier gas. Using the known outer diameter of the torch outer tube (D = 20 mm) and its corresponding pixel dimension in the image, the spatial resolution of the camera was calibrated to be 27.58 μm/pixel. By adjusting the aperture and shutter parameters, clear motion trajectories of the ion clouds generated from Er_2O_3 particles were successfully captured. Subsequently, the torch was rinsed with 2% HNO_3 solution followed by ultrapure water to eliminate residual Er_2O_3. The camera spatial resolution was recalibrated, yielding a value of 28.62 μm/pixel. A Y_2O_3 suspension was then nebulized, and the motion trajectories of the corresponding ion clouds were recorded. The cleaning, calibration, and nebulization procedures were repeated to obtain trajectory images for borosilicate glass particles with nominal diameters of 10 μm, 5 μm, and 2 μm. To improve positioning accuracy, the particle positions in consecutive frames were manually identified. To enhance processing efficiency, dedicated code was developed based on the MATLAB Image Processing Toolbox to assist in batch extraction of particle positions. The particle velocities were finally calculated from the displacement between two consecutive frames divided by the corresponding time interval.

The ion cloud trajectories corresponding to different particles are shown in **Figure 6**. The elongated streaks observed in the images result from motion blur caused by the limited frame rate of the camera. In velocity calculations, the center position of each ion cloud was extracted, and the velocity was determined by averaging the displacement over five consecutive frames. This approach effectively reduced the influence of motion blur on positioning accuracy, ensuring the reliability of the obtained velocity data.

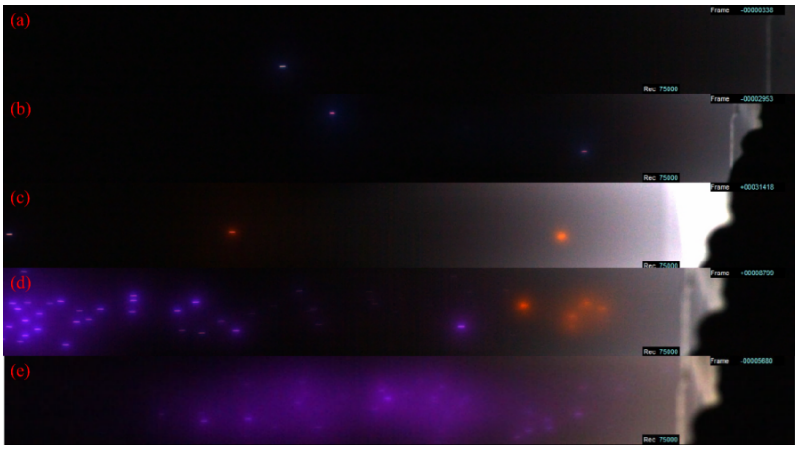

Figure 6. Experimentally captured ion cloud trajectories of different particles in the ICP tail flame: (a) Er_2O_3, (b) Y_2O_3, (c) BSG_10, (d) BSG_5, and (e) BSG_2.

In high-speed imaging observations, tracer particles with different chemical compositions exhibited distinct emission characteristics in the ICP tail flame, which directly affected their suitability as flow tracers. As shown in **Figure 6b**, the nebulized Y_2O_3 particles underwent evaporation, ionization, and excitation in the high-temperature plasma, forming stable pale pink luminous clusters. This color originates from characteristic emission lines of neutral or singly ionized yttrium species, Y(I) or Y(II). In contrast, Er_2O_3 particles displayed bright white emission (**Figure 6a**), which is closely associated with the rich emission spectrum of erbium. The emissions of both particle types were stable and persistent, forming clear motion trajectories suitable for subsequent velocity calculations. The borosilicate glass particles used in this study are multicomponent systems primarily composed of B_2O_3-SiO_2, with additional oxides such as Na_2O and K_2O. As shown in **Figure 6c–6e**, the observed yellow and purple emissions mainly originate from Na and K spectral lines, respectively.

The motion trajectories of ion clouds generated from injected particles were successfully recorded. For each particle type, the axial position (z) and radial position (r) of 60 ion clouds at different time instants were extracted to calculate the axial velocity V_z. The polynomial fitting curves of V_z versus axial position for different particles are presented in **Figure 7**.

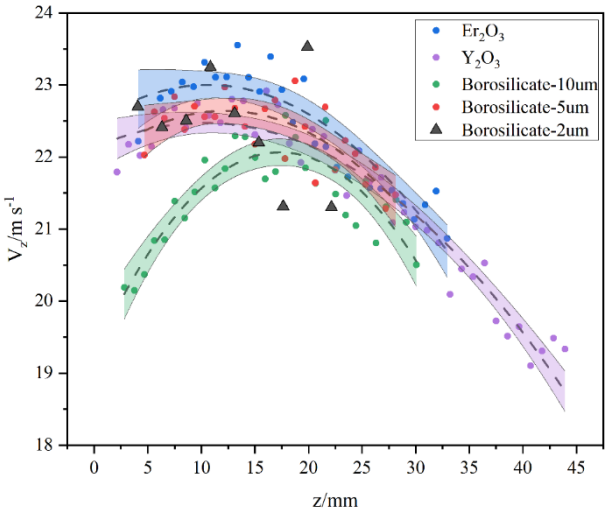

Figure 7. Axial velocity distributions of different particles in the ICP tail flame.

As shown in **Figure 7**, the measurements for Er_2O_3 and Y_2O_3 particles indicate that within the axial range of z = 2.5–12.5 mm, the velocity remains at a high plateau. This region corresponds to the standard analytical zone commonly used in ICP-MS or ICP-OES, where flow stability plays a crucial role in sample transport efficiency. In the downstream region (z > 12.5 mm), the velocity decreases significantly due to momentum dissipation caused by entrainment of surrounding air. The axial velocity of 10 μm borosilicate glass particles (BSG_10) is slightly lower than that of the other four particle types.

To ensure the accuracy and stability of velocity measurements in subsequent parametric studies (e.g., varying RF power or sample gas flow) and to maintain comparability across different experimental conditions, Y_2O_3 particles were selected as the standard tracer for all following experiments.

3.3. Effects of varying parameters on the axial velocity distribution in the ICP tail flame

3.3.1. The RF power

With the sample gas flow rate fixed at 1 L/min, the RF power was varied from 900 to 1300 W. The motion

trajectories of ion clouds generated from nebulized Y_2O_3 particles were recorded, and the corresponding axial velocity distributions V_z are shown in **Figure 8**. The measured increases with RF power at all axial positions, indicating enhanced jet momentum with higher energy input. In the downstream region (z > 12.5 mm), V_z decreases gradually with axial distance due to jet expansion, turbulent mixing, and momentum dissipation in ambient air.

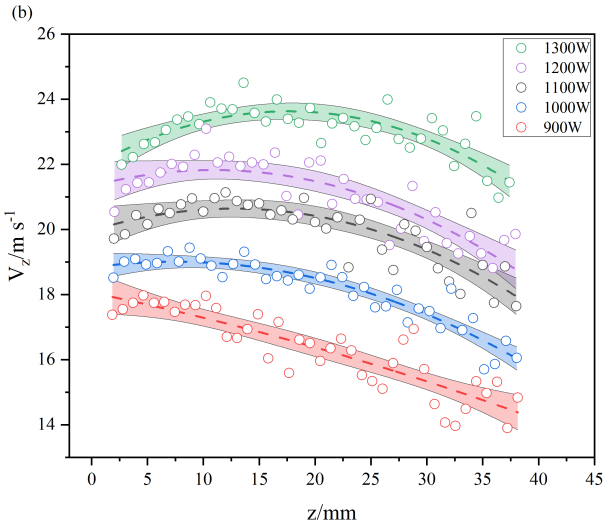

Figure 8. Axial velocity distributions along the plasma centerline under different RF powers.

As shown in **Figure 9**, under RF power of 1200 W and a sample gas flow rate of 1 L/min, the linear velocity distribution obtained in previous work over the axial range of 12.5–85 mm from the torch outlet is compared with the results measured in the present study over 0–40 mm.

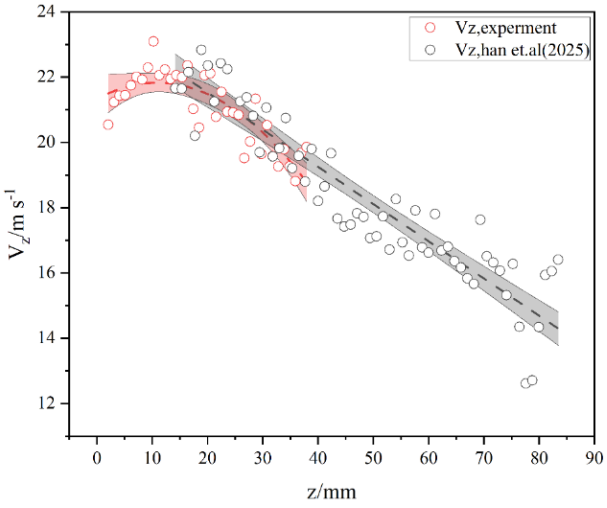

Figure 9. Comparison of axial velocities in the ICP tail flame between Han *et al.* and the present study.

A polynomial fit of the experimental V_z data in the present study yields:

$$V_z = 21.7 + 0.133z - 0.003\,z^2 \quad (2)$$

In comparison, the linear fit from previous work over the axial range of 12.5–85 mm is [12]:

$$V_z = 23.8 - 0.114\, z \quad (3)$$

At z = 12.5 mm, the fitted value in this study is 22.89 m/s, which is in good agreement with the previous value of 22.38 m/s (relative deviation ≈ 2.3%). This indicates good consistency between the two datasets in the overlapping measurement region and validates the reliability of the present experimental method.

Taking the case of RF power at 1200 W as an example, the experimentally measured axial velocity distribution of particles was fitted and compared with the particle trajectory evolution obtained from numerical simulations by Mostaghimi *et al.* as well as the simulated curves from the 2D model at different powers, as shown in **Figure 10** [11]. The results indicate that, consistent with Mostaghimi's conclusions, the particle axial velocity exhibits a clear plateau in the downstream region of the torch outlet over the axial range of 2.5 mm < z < 12.5 mm.

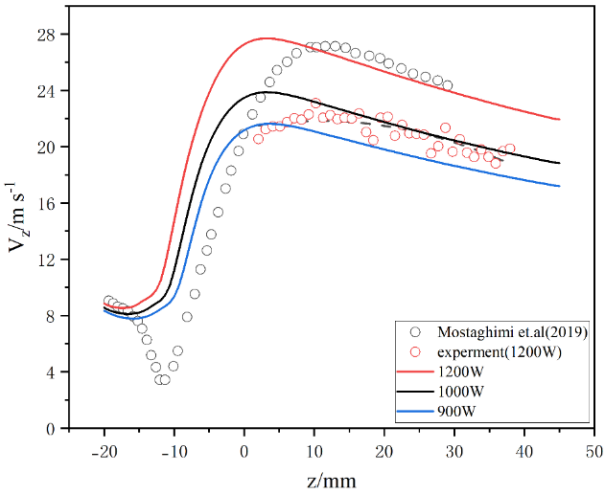

Figure 10. Axial particle velocities in the ICP tail flame: Comparison between experimental measurements, polynomial fit, and simulations.

This velocity plateau region generally corresponds to the Normal Analytical Zone (NAZ) of the plasma and is closely associated with the relatively high and stable central temperature distribution within this region. As the axial distance increases further, both particle and gas axial velocities gradually decrease due to the progressive entrainment of ambient air and the continuous dissipation of momentum and energy.

3.3.2. Sample flow rate

Under a fixed RF power of P = 1200 W, the sample gas flow rate was set sequentially to 1.2, 1.0, 0.8, 0.6, and 0.4 L/min. Using the same processing method as for the varying-power experiments, the axial velocities (V_z) were calculated. **Figure 11** presents the polynomial fits of the centerline velocities for different sample gas flow rates, along with the corresponding centerline velocity curves predicted by the 2D numerical model for the same flow conditions.

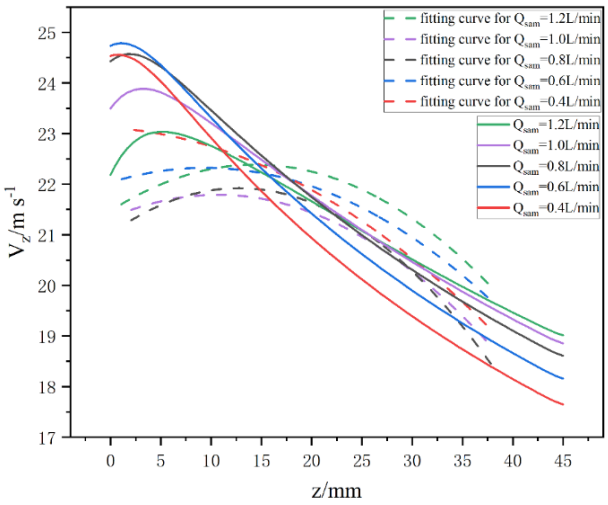

Figure 11. Comparison of experimental and simulated centerline velocity distributions at different sample gas flow rates in the ICP tail flame.

Figure 11 shows that the measured axial velocity distributions in the ICP tail flame at different sample gas flow rates indicate a limited influence of flow rate on the overall velocity level. This suggests that in the near-field region of the tail flame close to the torch outlet, the axial flow is primarily driven by gas expansion and pressure gradients induced by plasma heating, rather than by the cold gas volumetric flow itself.

Notably, in the region $z < 12.5$ mm, the axial velocity measured at lower flow rates is slightly higher than that at higher flow rates. Under a constant RF power, a smaller gas flow implies higher heating power per unit mass, leading to an increased core plasma temperature and stronger gas expansion, which enhances axial jetting. Conversely, at higher flow rates, the additional cold gas entering the plasma region exerts a cooling and dilution effect on the hot core, reducing near-field acceleration and lowering the axial velocity peak.

Therefore, in the near-field region of the ICP tail flame, axial velocity is far more sensitive to RF power than to sample gas flow rate. The higher near-field velocities observed at lower flow rates further confirm that flow in this region is dominated by thermal driving effects.

4. Conclusion

In this work, a custom ICP source was employed, and the axial velocity in the tail flame within the normal analytical zone (NAZ) of the plasma was directly measured using a high-speed camera. The particle tracing method was systematically applied to investigate the effects of different tracer particles and plasma operating conditions on the axial velocity distribution in the ICP tail flame. Compared with previous work, the present study provides experimental velocity data for the region close to the torch outlet ($z < 12.5$ mm), filling a gap in the characterization of near-field plasma flow. The results show that a clear velocity plateau along the plasma axis (V_ z distribution) can be observed in both experimental measurements and numerical simulations, consistent with the particle trajectory simulations of Mostaghimi *et al.*, thus validating the reliability of the experimental method and the measured data. These findings offer direct experimental evidence for a deeper understanding of the dynamic flow behavior in analytical ICPs and provide critical reference data for the development and validation of numerical models. The observed velocity distributions and their response to operating parameters are of significant

importance for optimizing ICP analytical conditions and enhancing the predictive capability of numerical simulations for real plasma behavior.

Disclosure statement

The authors declare no conflict of interest.

References

[1] Montaser A, 1998, Inductively Coupled Plasma Mass Spectrometry, John Wiley.

[2] Boss C, Fredeen K, 1997, Concepts, Instrumentation and Techniques in Inductively Coupled Plasma Optical Emission Spectrometry, Perkin-Elmer, Second.

[3] Tsivilskiy I, Gilmutdinov A, Nikiforov A, et al., 2020, An Experimentally Verified Three-Dimensional Non-Stationary Fluid Model of Unloaded Atmospheric Pressure Inductively Coupled Plasmas, J. Phys. D. Appl. Phys., 53(2020): 455203.

[4] Nagulin K, Akhmetshin D, Gilmutdinov A, et al., 2015, Three-Dimensional Modeling and Schlieren Visualization of Pure Ar Plasma Flow in Inductively Coupled Plasma Torches. J. Anal. At. Spectrom., 2015(30): 360–367.

[5] Nagulin K, Tsivilskiy I, Akhmetshin D, et al., 2017, Transient Three-Dimentional Dynamics of Argon Plasma within the Vacuum Interface of the Inductively Coupled Plasma Mass Spectrometer System. Spectrochima Acta Part B: At. Spectrosc., 2017(135): 63–72.

[6] Colombo V, Ghedini E, Mostaghimi J, 2008, Three-Dimensional Modeling of an Inductively Coupled Plasma Torch for Spectroscopic Analysis. IEEE Trans. Plasma Sci., 2008(36): 1040–1041.

[7] Gamez G, Lehn S, Huang M, et al., 2007, Effect of Mass Spectrometric Sampling Interface on the Fundamental Parameters of an Inductively Coupled Plasma as a Function of its Operating Conditions: Part II. Central-Gas Flow Rate and Sampling Depth. Spectrochim Acta Part B: At. Spectrosc., 2007(62): 357–369.

[8] Huang M, Hanselman S, Yang P, et al., 1992, Isocontour Maps of Electron Temperature, Electron Number Density and Gas Kinetic Temperature in the Ar Inductively Coupled Plasma Obtained by Laser-Light Thomson and Rayleigh Scattering. Spectrochim Acta Part B: At. Spectrosc., 1992(47): 765–785.

[9] Ebert C, Saetvit N, Bajic S, et al., 2020, High-Speed Photographic Study of Vaporclouds from Wet Droplets and the Subsequent Solid Particles in an Inductively Coupled Plasma. J. Anal. At. Spectrom., 2020(35): 1956–1958.

[10] Aeschliman D, Bajic S, Baldwin D, 2003, Spatially-Resolved Analysis of Solids by Laser Ablation-Inductively Coupled Plasma-Mass Spectrometry: Trace Elemental Quantification without Matrix-Matched Solid Standards. J.Anal. At. Spectrom., 2003(18): 1008–1014.

[11] Guo X, Alavi S, Dalir E, et al., 2019, Time-Resolved Particle Image Velocimetry and 3D Simulations of Single Particles in the New Conical ICP Torch. J. Anal. At. Spectrom, 2019(34): 469–479.

[12] Han X, Su Y, Li Z, et al., 2025, Experimental Study on the Dynamic Characteristics of an Analytical Inductively Coupled Plasma and its Tail Flame. Journal of Analytical Atomic Spectrometry, 2025(40): 1916–1928.